Spatial Structure Formation in Precipitation Reactions

Stefan C. Müller[†] and John Ross*[,‡]

Institut für Experimentelle Physik, Otto-von-Guericke-Universität Magdeburg, Universitätsplatz 2, D-39106 Magdeburg, Germany, and Department of Chemistry, Stanford University, Stanford, California 94305-5080

Received: March 24, 2003

We analyze selected experiments on spatial structure formation in the presence and the absence of imposed gradients of concentrations, with emphasis on length scales, time scales, initial degree of supersaturation, and initial concentration differences of the ions forming the precipitate. In relation to these experiments, we discuss two major proposed models. The first is the Ostwald−Prager model of Liesegang bands for systems with imposed concentration gradients (diffusion of ions occurs and at a given degree of supersaturation, nucleation and precipitation to form bands take place discontinuously but repeatedly in space) The other model, known by various designations (Ostwald ripening, competitive growth model, Turing instability) for systems with and without imposed gradients, supposes nucleation to occur continuously in a region of space, followed by the competitive and autocatalytic growth of larger particles at the expense of the dissolution of smaller particles within that region of space. This process coupled to diffusion may lead to macroscopic Turing structures. We find extensive experimental evidence for the second model over a large range of initial concentrations of electrolytes as well as some theoretical evidence, and we find the experimental evidence presented for the validity of the first model alone to be insufficient.

I. Introduction

Many articles have been reported on structure formation in precipitation reactions: the topic includes Liesegang rings[1] observed in the presence of concentration gradients and structure formation in the absence of such gradients, including Turing structures.[2,3]

Substantial experimental results have been reported, and there are categories of different theories. It is no surprise that there is some disagreement and confusion on nomenclature as well as on the interpretation of some of the results. This field may have suffered from its apparent simplicity; however, the subtleties of the subject have led to more than a century of ongoing investigations and discussions.

In this article, we analyze some pertinent experiments on this topic with systematic emphasis on length scales, time scales, initial degree of supersaturation, S, concentration differences, Δ, of the ions forming the precipitate, and whether the structure formation is due to either nucleation and precipitation occurring essentially at the same time discontinuously in space (Ostwald−Prager or OP model[4,5−9]) or a post-nucleation phenomenon (nucleation occurring continuously in space), which may involve instabilities coupled with diffusion (TI model[3,4,10−14]). We find that this analysis provides a useful ordering and possible distinctions among various experiments and shows the limitations of several theoretical models. Our work provides some new insights and clarifications, and on the basis of our analysis, we find the experimental evidence for the OP model to be insufficient.

Typical Liesegang patterns are observed when a weakly soluble salt is produced from the reaction of two soluble substances, for instance,

$$NH_4OH + MgSO_4 \leftrightarrows Mg(OH)_2 + ...$$

or

$$2KI + Pb(NO_3)_2 \leftrightarrows PbI_2 + ...$$

Experiments are usually performed either in a test tube or in a Petri dish. In the first case, a solution of one of the reacting substances in placed above the solution of the other, containing a gel to prevent convection and sedimentation. Subsequently, in the area of interdiffusion, the formation of a precipitating salt starts. The spatial distribution of the precipitate depends on the initial concentrations of the source substances, and very often the precipitate is distributed inhomogeneously in space, forming bands parallel to the diffusion front that are separated by distinct spacings, as shown in the example of Figure 1A.[15]

In a Petri dish, a succession of concentric rings of precipitate can appear if a solution of one of the source reactants is added to the center of the dish already containing the solution of the other reactant. If the initial concentration of the electrolyte at the center is substantially higher than that of the second electrolyte (i.e., the concentration difference, Δ, is large)[16] and if the initial degree of supersaturation, S, is sufficiently high, then a reaction front begins to move from the center to the periphery of the dish as a result of diffusion of the added substance, leaving behind well-separated rings of precipitated salt. This was first shown and systematically studied by R. E. Liesegang in a system producing concentric rings of silver dichromate in a thin layer of gelatin[17] (Figure 1B) and was afterward reported for many other slightly soluble electrolytes.[18,19] Although a gel is not essential for banded precipitation to occur, as shown soon after the discovery of this phenomenon,[20] its presence may influence the details of the structure formation process. Bands may be produced even in the solid[21]

* Corresponding author. E-mail: john.ross@stanford.edu. Phone: 650-723-9203. Fax: 650-723-4817.
[†] Otto-von-Guericke-Universität Magdeburg.
[‡] Stanford University.

10.1021/jp030364o CCC: $25.00
Published on Web 09/10/2003

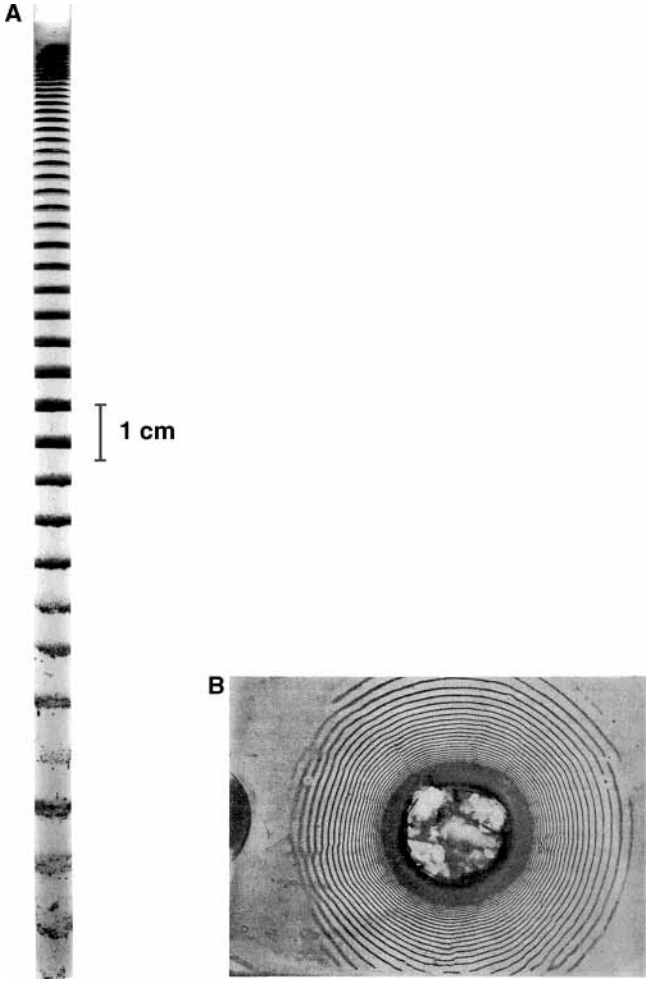

Figure 1. (A) Parallel bands of precipitated lead iodide in agar gel (1%) with initially 240 mM KI in the upper and 9 mM $Pb(NO_3)_2$ in the lower portion of a tube. Scale bar: 1 cm. (B) Ring-shaped periodic precipitation of silver dichromate in a thin layer of gelatin gel, as reported by R. E. Liesegang in one of his earliest photographs taken in 1896 (from ref 17).

or gas phase[22] and have been found on a micrometer scale in water-swollen polymer films.[23] Certain geological formations that display spatial rhythm may have formed by the diffusion of salts through a gellike matrix (cf. Chapter 13 in ref 1f), and some biological or biomedical structures are likely to be caused by a similar mechanism (e.g., gall stones,[24] urinary calculi, or mucus around cancer cells).

In most systematic experiments, the two reactants are placed in a narrow test tube, which confines the direction of diffusion to essentially one spatial coordinate, resulting in a 1D structure (Figure 1A). The frequently observed regular and reproducible bands of deposited precipitate have been described in terms of a simple spacing and time law[20,25] that relates the location x_n of the nth band to its time of formation t_n according to $x_n \approx t_n^{1/2}$ and describes successive locations by the quotient $x_n/x_{n+1} = p$, with p denoting a constant spacing coefficient. The width of the bands also increases with increasing distance from the interface,[26] and a corresponding power law has been formulated.[27]

There are, however, numerous reports on different pattern characteristics: these include the revert spacing reported in 1928[28] and further investigated in refs 3 and 29. Here the spacing decreases with increasing distance from the junction of the solution. Some studies have shown secondary structures, such as the separation of one band, once formed, into several closely adjacent thinner bands.[30,31] Quite frequently, under apparently the same experimental conditions, "curiosities"[32] are observed such as radially aligned gaps[31] or zigzag-shaped dislocations of the ring structure in a Petri dish,[33] spirals or helices instead of a set of rings or bands,[34,35] or "Saturn rings" in a test tube.[6] A remarkable variety of structures have been reported recently in ref 36 with a phase diagram showing transitions between regular and irregular shapes of precipitation bands; the axes of this diagram are the initial concentrations of the interdiffusing reagents.

Macroscopic periodic structures may also arise from an electrolyte solution in the absence of any fields such as gradients of concentration or temperature or the gravitational field. For instance, if a solution of lead iodide is prepared at elevated temperatures, a gel-forming substance is added to the solution, and the solution is allowed to cool slowly; then a uniform nucleation of colloidal lead iodide is induced at sufficient supercooling, and precipitation occurs inhomogeneously in irregular patterns with length scales ranging, in general, from 0.5 to 10 mm.[10,11,37] In ref 38, examples are reported that can be roughly characterized as a 2D network, a wavelike structure reminiscent of Liesegang rings, and a speckled pattern.

To explore the full range of structure formation from initially large concentration gradients (the classical Liesegang case) to low and vanishing initial gradients, we have made a systematic study of Liesegang ring formation and the dependence of their number, locations, and widths on Δ and S.[26,38] For definitions of S and Δ see Section II. The range of S investigated goes from 17 to 10^{13}, and that of $|\Delta|$ from 0 to 7 M. As either Δ is decreased to zero or S reaches a lower critical limit, band formation becomes increasingly stochastic in the formation and placement of the rings. There is a continuity in structure formation from zero to increasing concentration gradients that has led to the suggestion that the origin of pattern formation is the same in all cases.[12]

During the past decade, a number of authors have studied the effects of externally imposed fields on the onset and evolution of precipitation bands. For this purpose, electric fields[39] and light[40] have been used. Other recent work focuses on details of the morphological characteristics using microdensitometric and microscopic techniques to elucidate the properties of a moving nucleation front that establishes a subsequent turbidity zone in which rings of silver chromate/dichromate subsequently form.[41,42]

Many theories have been proposed for a mechanistic explanation of patterned precipitation. Stern summarizes in his review[43] of the Liesegang phenomenon the theoretical approaches developed until 1954, and Henisch presents a thorough overview of publications that have appeared on that issue until 1991.[1e] In addition to the theories based on Ostwald's supersaturation hypothesis mentioned above (OP model[4]) and a number of approaches that turned out not to be supported by experimental observations, an early suggestion for a postnucleation scenario was made in the "coagulation theory",[44] which assumes that precipitation bands arise by coagulation (or flocculation) of the colloid if certain critical electrolyte concentrations are exceeded. This theory alone cannot convincingly explain the creation of large clear regions between bands on long time scales. From the early 1970s onward, the role of competitive and autocatalytic particle growth in structure formation in the postnucleation phase involving instabilities was discussed in the literature (TI model[4]) to explain the rich morphologies observed through the years in preciptation patterns in systems with and without macroscopic

TABLE 1: Characterization of Selected Experiments on Structure Formation in Precipitation Reactions

no.	chemical system	ref no. (year)	conc	gel (%)	time scale	type of structure (geometry)	length scale	S	Δ (mM)	T (°C)	comments
						A. No Initial Gradient					
1	lead iodide	3 (1974)	KI 9 mM $Pb(NO_3)_2$ 2.25 and 4.5 mM	agar, 0.5 1	12−24 h	Turing type (test tube, diameter 5−10 mm)	1 cm 1 mm−1 cm	17.2	0 for initial sol	20	KI and $Pb(NO_3)_2$ initially mixed to form PbI_2
2	lead iodide	10 (1978)	PbI_2 4.5−5.9 mM	agar 1	30−80 min	speckle, mosaic (layer in Petri dish, 1.5 mm thick)	2 mm −cm	26−60	0	room	Patterns obtained in supercooled PbI_2 in agar gel
			KI 60 mM $Pb(NO_3)$ 30 mM	agar	1−4 h	"open" system (layers 5 mm thick)	1 mm	7770	0		reaction layer sandwiched between KI and $Pb(NO_3)_2$ layers (plate V in ref 10)
3	lead iodide	37 (1982)	PbI_2 4.8−6.6 mM	agar 1	<1 week	network, mosaic, layer in Petri dish, 1 mm thick	2−8 mm and 0.5−2 mm	32−83	0	25	measured size distributions of colloidal particles
4	lead iodide	51 (1994)	PbI_2 5.2−7.0 mM	agar 1		Swiss cheese network	same as in 3	40−100	0		
5	lead iodide	52 (1987)	KI 93 mM $Pb(NO_3)_2$ 500 mM	agar	14 s−15 min	network, greedy giants; observation in one band extending across a square cell	0.3 mm	3×10^5	0		pattern in plane parallel to diffusion front in a Liesegang experiment (system A3 of ref 53)
						B. Small Imposed Gradient					
6	lead iodide	53 (1973), 3 (1974)	PbI_2 *sol* from KI 9 mM $Pb(NO_3)_2$ 2.25 mM KI 0.9−9 mM (on top)	agar 0.5	days	faint bands of irregular spacing; no or reverse gradient in thin tube	cm		negative	20	ref 54, Figures 5 and 11; Note: Figure 3 mentioned in section IIIA2 of ref 3 should be Figure 5 in ref 54 (same as Figure 6 in this article). The photograph shown in ref 3 is Figure 12 in ref 54, as mentioned correctly in section IIIA3 of ref 3: no reverse gradient, but gradient in a sol.
						C. Intermediate and High Imposed Gradients					
7	lead iodide	26 (1982)	KI 6−170 mM $Pb(NO_3)_2$ 3−100 mM	agar 1	20 days	I: critical lower limit for bands at $S = 200$; deviations from spacing law for low S	1 mm− 1 cm	(170− 3) × 10^4	15, 30 (*kept constant*)	room	
						II: changes in number, spacing, width	0.5− 3 cm	(500− 2.3) × 10^4	0−50 pos. and neg.		II: many morphological details; effects of different diffusivities
					2 days− 1 month	III: bifurcation with change in Δ	2 mm− 1 cm	500−1300 (*kept constant*)	0−30		III: sequence in Figure 1 of paper: $S = 1300$, $\Delta = 2.6-25$
8	lead iodide	38 (1983)	KI 14−70 mM $Pb(NO_3)_2$ 1.7−17 mM	agar 1	16−24 h	continuous yellow zone; ring develops within this zone	1-mm band in 1-cm zone	1007	9	room	
					3 weeks	stochastic placement of rings with $\Delta \rightarrow 0$; in tubes of diameter 5 mm	1−3 cm	1000−1300	0		
9	lead iodide	56 (1987)	KI 300 mM $Pb(NO_3)_2$ 15 mM		4 days	ring splitting, secondary structure	5 mm	10^5	135		exp from S. Kai et al., named "subring" formation
10	magnesium hydroxide	57 (1982)	NH_4OH 5.5 M $MgSO_4$ 0.4 M	gelatin 9	2 h (1 ring) 28 h (3 rings)	pH, turbidity front, focusing effect (thin tubes, diameter 5 mm)	1−5 mm	10^{12}	2.35 M	22	

TABLE 1 (Continued)

no.	chemical system	ref no. (year)	conc	gel (%)	time scale	type of structure (geometry)	length scale	S	Δ (mM)	T (°C)	comments
11	silver dichromate	41 (1993)	$AgNO_3$ 10M $K_2Cr_2O_7$ $10^{-4}-0.2$ M	gelatin 15		turbidity front	0.2−0.5 mm	$10^8-2\times10^{11}$	5 M		microdensitometry
12	lead iodide	52 (1987)	$Pb(NO_3)_2$ 0.5 M KI 0.01−0.093 M and more combinations	agar	3 rings in 40 min, 10 rings in 800 min	square box (10 cm × 10 cm^2) with 5-mm gel layer		4.2×10^3 (A1); 1.7×10^4 (B1)	−445 (A1) 95 (B1)	20	taken from Figure 2 (system A1) and Figure 3 (system B1) in ref 53
13	magnesium hydroxide	59 (1962)	NH_4OH 14.8 M	gelatin	4 h (1 ring)	afterward cut into slices and analyzed (tube, diameter 5 mm)	8 mm	3.8×10^{13}	7.07 M	28	similar series with agar
			$MgSO_4$ 0.33 M $MgSO_4$ 0.45 M		22 h (2 rings)		2 mm		6.95 M	3	

gradients. The occurrence of some of the complex structural features, such as dislocations and helices, has been successfully reproduced by numerical simulations based on the assumption that for the formation of precipitation patterns both the periodic supersaturation and the following dissolution of small particles and the growth of large particles (Ostwald ripening) are essential.[45] The role of fluctuations in the nucleation process of colloidal particles has been considered by cellular automata.[46] A spinodal decomposition model for Liesegang patterns, which reproduces the spacing law and the dependence of the spacing coefficient p on the concentrations of the interdiffusing electrolytes, was suggested.[47]

We return to the issue of theories in the Discussion section. In the following text, we will present an analysis of some selected experiments (section II). Section III has a brief discussion including comments on some recent theories and, section IV offers suggestions for future experiments.

II. Analysis of Some Selected Experiments

In Table 1, we list selected experiments on structure formation in precipitation reactions. For each entry, we provide the following information: the chemical system, the reference number and year of the experiment, the initial concentrations of the chemical species, the times of observations of the structure formation (the time scale), the types of structures formed, the length scale of the structure formation, and the initial degree of supersaturation. For example, $S = [Pb^{2+}][I^-]^2/K_{sp}$ for lead iodide, where [X] is the concentration of X and K_{sp} is the solubility product. The initial ion concentration difference $\Delta = {}^1/_2[I^-] - [Pb^{2+}]$; the temperature and comments are also listed.

Section II.A lists experiments with initially uniform concentrations in the system; section II.B, experiments with small imposed concentration gradients; and section II.C, experiments with intermediate and large imposed concentration gradients, each in order of increasing S.

A. No Initial Gradients; Initially Uniform Systems.

1. Lowest $S = 17.2$. In experiments reported in ref 3, line 1 in Table 1, a supersaturated solution of PbI_2 and agar in a test tube is initially uniform. After a few hours, there appears a uniform yellow haze due to the formation of very small colloidal particles. The total concentration (particles and ions) as tested is uniform. After 12−24 h, macroscopic structure formation occurs reproducibly on a length scale of centimeters—there are regions of lighter and darker colors of yellow precipitate (Figure 2). The particles are of a size (micrometers) such that their diffusion in agar is negligible. These experiments indicate time-dependent Turing structures. (See refs 2 and 3, and for time-independent Turing structures, refs 48−50.) We follow Turing's nomenclature[2] in the use of the designations of "time-dependent" and "time-independent" structure. (See also ref 12.) As the colloidal particles grow, some grow faster than others; the concentration of electrolytes in equilibrium with larger particles is lower than that in equilibrium with smaller particles. An electrolyte concentration gradient is established such that the electrolyte diffuses from the smaller to the larger particles, which leads to the autocatalytic growth of the larger particles at the expense of the smaller particles, a process called Ostwald ripening. This process coupled with the diffusion of the electrolyte may lead to a Turing bifurcation and structure formation.[3,10,11] In the denser regions of the colloid, there was not seen by visual inspection evidence for a substructure, but no microscopic examinations were made.

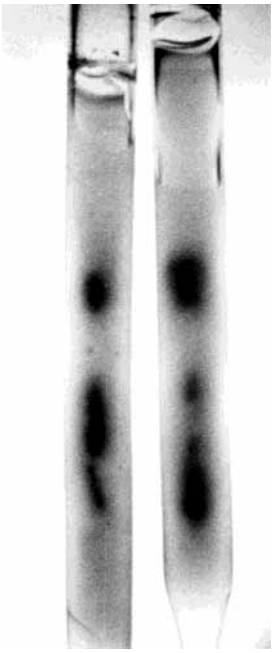

Figure 2. Inhomogeneous macroscopic structures formed from initially homogeneous supersaturated solutions of lead iodide in agar gel (1%). Initial concentrations: 4.53 mM $Pb(NO_3)_2$, 18.07 mM KI, 1% agar. Tube diameter, 5 mm (from ref 3).

2. Intermediate S. In several studies (refs 10, 37, and 51, lines 2−4 in Table 1), structure formation in initially homogeneous systems has been investigated in the geometry of a thin layer (about 1 mm) of an electrolyte in a gel. For example, a solution of PbI_2 and agar at an elevated temperature is poured into a Petri dish; when the system has cooled to 22 °C, a gel has

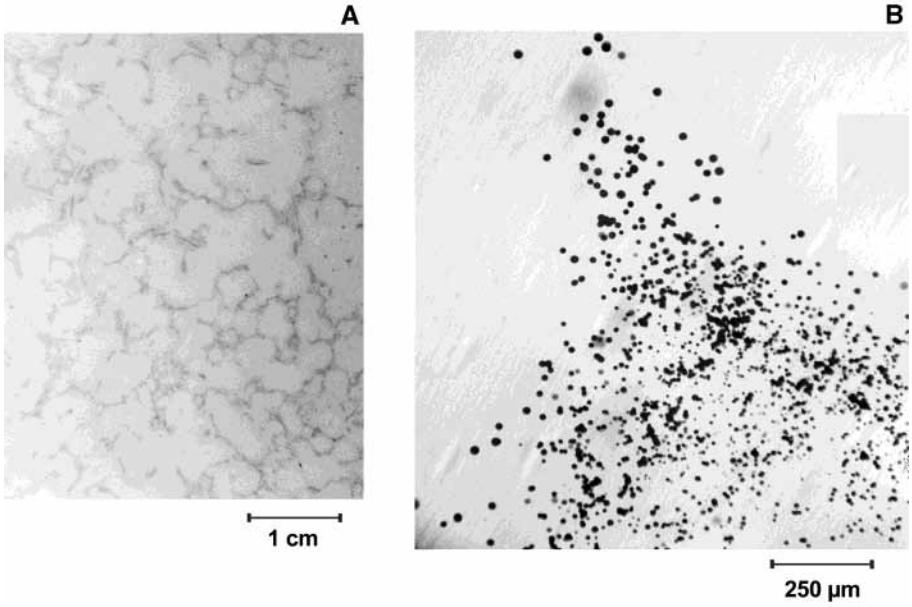

Figure 3. Precipitation pattern of lead iodide in agar gel without initially imposed gradients of concentration. The system was prepared at an elevated temperature in a Petri dish of diameter 90 mm with a layer thickness of 1.5 mm. Initial concentrations: 5.2 mM PbI_2, 1% agar. The pattern evolved at 22 °C and is shown after 1 week. (A) Photograph of macroscopic inhomogeneities and (B) microscope photograph of a part of A (from ref 37).

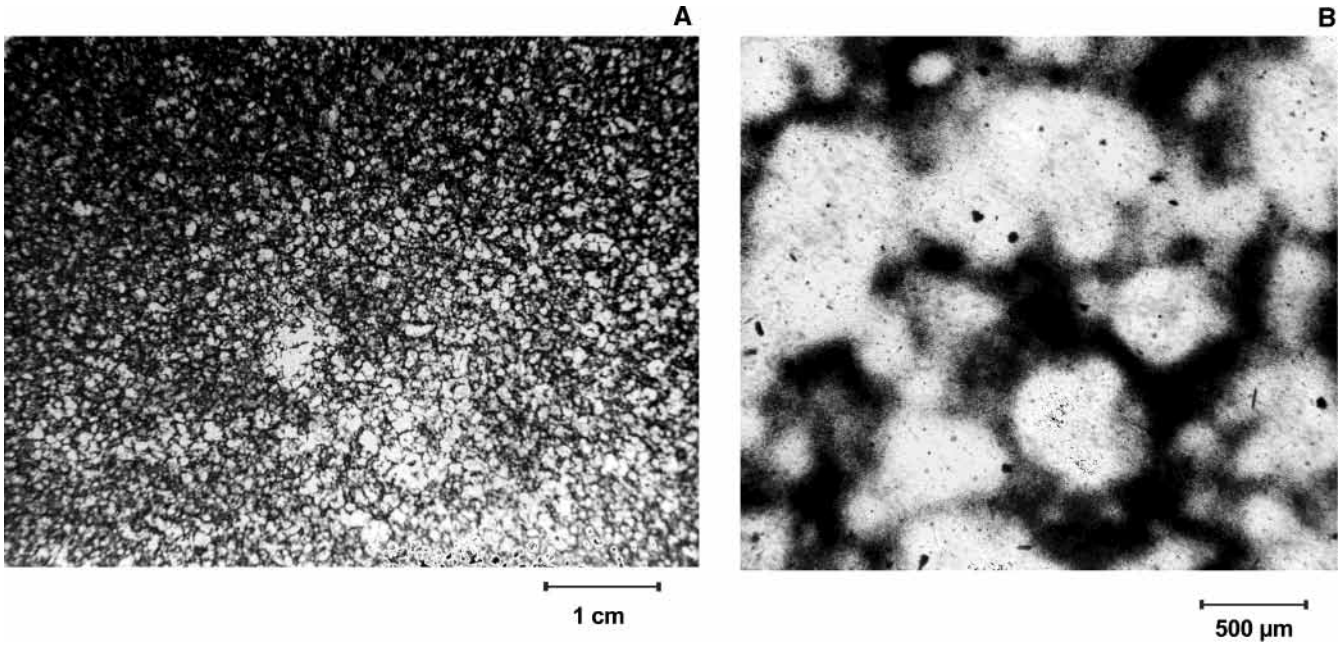

Figure 4. Precipitation pattern of lead iodide in agar gel without initially imposed gradients of concentration, as shown in Figure 3 but with initial concentrations of 6.4 mM PbI_2 and 1% agar. (A) Photograph of macroscopic inhomogeneities and (B) microscope photograph of a part of A (from ref 37).

formed that within an hour begins to turn uniformly yellow, like a haze. Nucleation has taken place, and a colloid consisting of small particles of PbI_2 has formed. The gel then is still relatively transparent, hence the average particles size is less than the wavelength of light.[10] After several more hours, nonuniformities in colloid concentration appear and develop into macroscopic structures. A typical pattern obtained with an initial value of $S = 22.6$ is shown in Figure 3, and that with an initial value of $S = 42.7$, in Figure 4. The initial concentrations differ only by about 20%: 5.2 and 6.4 mM. In view of this, the substantial difference in the space filled by particles in Figures 3A and 4A is at first surprising. However, the difference in the average size of the small colloidal particles in these two cases is substantial: 4.3 μM in Figure 3B and 0.8 μM in Figure 4B. A simple calculation in Appendix A shows that because of this size difference but at nearly the same concentrations the number of particles in Figure 4B is substantially larger and their projection onto the plane of the gel fills that much more space.

Within the spaces empty of colloidal particles, there are seen particles larger than the average size, named greedy giants by Ortoleva and observed in his studies of similar cases.[1f,3,37] These larger particles may have formed on heterogeneities, or they may have been formed in homogeneous nucleation by a fluctuation of rare occurrence. The experimental results shown in Figures 3B and 4B were made with the same source of distilled water, PbI_2, and agar. The number of large particles in empty regions in Figure 3B is much smaller than that in Figure 4B, suggesting that if the large particles in Figure 3B are formed

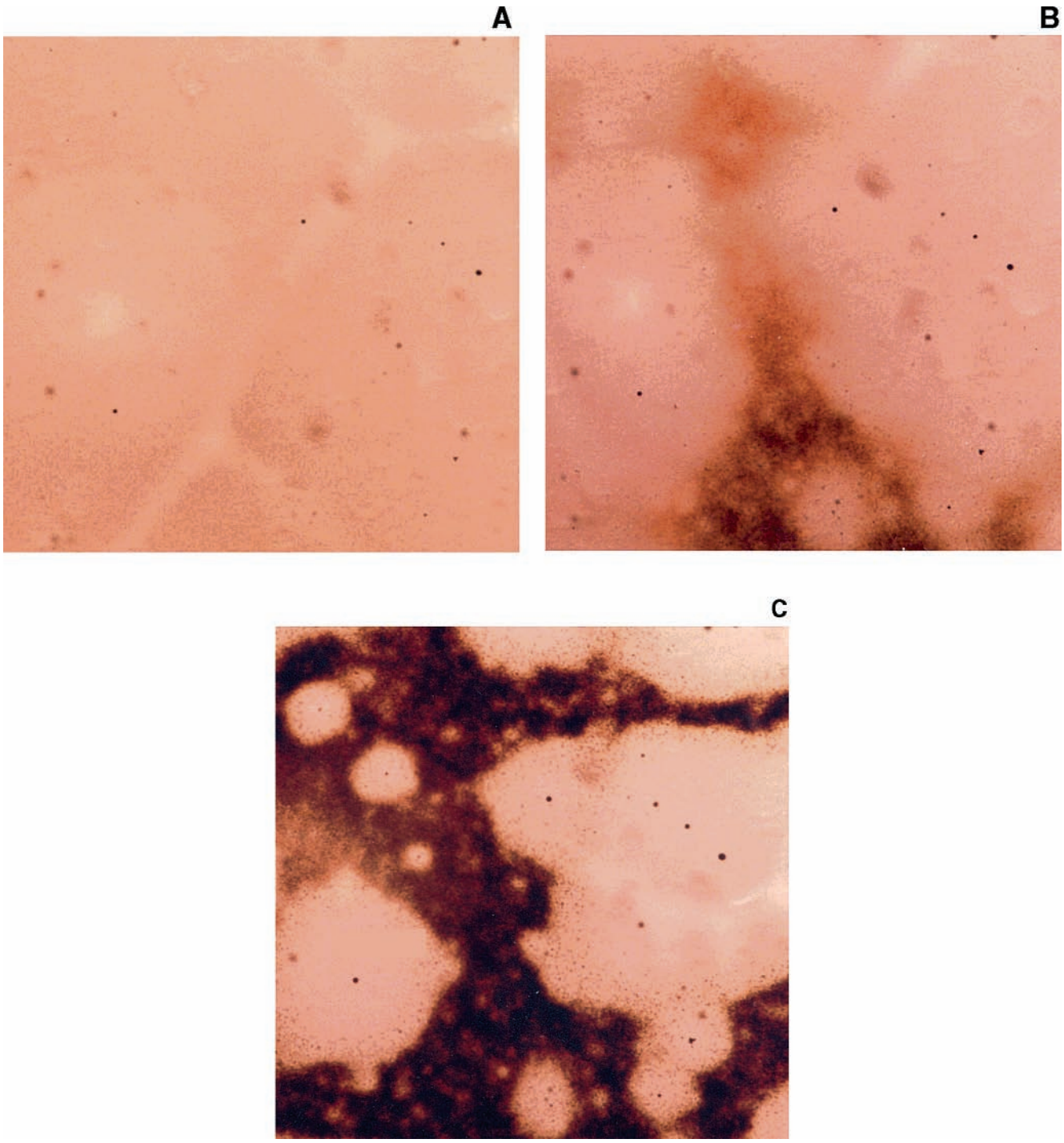

Figure 5. Microscope photographs (magnification 30×) of the temporal development of a precipitation pattern in a single band of PbI_2 formed from solutions with initial concentrations of 0.093 M KI and 0.5 M $Pb(NO_3)_2$ ($S = 3 \times 10^5$). Times after the start of the experiment: (A) 660 s, (B) 690 s, (C) 900 s (from ref 52).

by nucleation on heterogeneous particles then most of the larger particles in Figure 4B are due to homogeneous nucleation because the density of heterogeneous particles in the two cases is expected to be nearly the same. We defer a discussion of the development of such structures to the next section.

3. High S. An experiment similar to those cited in the last section was reported in ref 52, line 5 in Table 1. Onto a gel layer of agar 0.5 cm high containing 0.093 M KI, a solution of 0.5 M $Pb(NO_3)_2$, again 0.5 cm high, was poured. The initial value of S was 3×10^5. About 11 min later, the formation of a single band of PbI_2 0.15 cm into the KI gel was observed. The development in time of this layer is shown in a few selected photographs (amplification 30×) in Figure 5. The homogeneous nucleation of small particles takes place at about 11 min, as determined by the observation of a yellow band (Figure 5A), and certainly prior to the extensive homogeneous nucleation shown in Figure 5C. There are a few much larger particles present in Figure 5A−C, and as mentioned in the previous section, these may be heterogeneous particles at the core that are growing via accretion of lead iodide electrolyte or they may be particles formed by rare nucleation events. In Appendix B, we make a simple estimate of the probability of nucleation. The estimate for the recurrence time of the nucleation of five molecules is 3 s, which indicates a likely possibility of nucleation because it occurs in all systems in sections II.A.2 and II.A.3. However the estimate for the recurrence time for

the formation of a larger nucleus, say 10 molecules, is already enormous, about 10^{21} s, hence the probability for that event is negligible. Therefore, the larger particles, quite different in size from all of the other particles, are likely heterogeneous cores on which the accretion of precipitate occurs. Because such accretion is proportional to the surface area of the precipitate particles, the heterogeneous cores (perhaps 0.1 μm) grow much more rapidly than the homogeneously formed nuclei of a few molecules. Hence, we conjecture that there may be a few heterogeneous centers in the light regions of Figure 5A and B. Note, however, in Figure 5C that close to the dark regions and protruding into the lighter regions there are visible many more smaller particles than the largest ones which must have grown from homogeneously nucleated particles in part by Ostwald ripening.

From the analysis in the last section and in this section, we conclude that the length scale of the observed spatial patterns depends on the initial concentrations and therefore *S*, on the possible presence of heterogeneities to some extent, and on the coupling of Ostwald ripening and the diffusion of ions generated by the dissolution of smaller particles.

B. Small Imposed Gradients. We now proceed to systems with small (section B) and intermediate and high (section C) imposed macroscopic gradients. Experiments show that in all such cases which have been investigated a colloid is formed prior to any indication of band formation. Within the continuously formed colloidal region, there arise spontaneously in time concentration gradients that lead to band formation. This sequence of events rules out supersaturation as being significant in band formation.

Consider placing a homogeneous sol (colloid) of PbI_2 in a gel into a test tube, and then place on top of that a solution of KI. The concentrations are listed in Table 1, line 6.[53] If all of the lead in the sol were in colloidal form, then the concentration of I^- ions in solution would be 0.45×10^{-2} M. Hence, in the case of the KI concentration on top of the sol with a lower concentration of I^- than 0.45×10^{-2} M, I^- diffuses out of the sol. This small imposed and reversed gradient leads to Turing structures with visible bands of yellow color substantially deeper than that of the sol (Figure 6). Because the colloid exists prior to the imposition of a gradient and there is a reduction in the concentration of I^- in the sol after the imposition of the gradient, structure formation cannot possibly occur by the OP model but occurs by a Turing instability (cf. refs 3, 10−14). The development of structure in the absence of supersaturation effects has also been induced by an external gradient created by the diffusion of I^- into the sol. (See Figure 3 in ref. 3; cf. also early work by Hedges and Henley.[28])

C. Intermediate and High Imposed Gradients. Liesegang ring experiments are usually made at higher concentrations, that is, higher values of *S* and Δ, but in most of these experiments only the number of rings and their time of appearance are counted and the ring spacings and widths are measured. We reanalyze and integrate several experiments in which more details have been reported previously, and we find some interesting results.

(1) Extensive studies of Liesegang ring formation are reported in refs 26 and 38 for PbI_2 and agar along with a series of values of *S* from 500 to 1500 as well as a series of values of Δ from 0 to 25 mM. No ring formation was observed for *S* below 200.[26] We single out two observations from this work (Table 1, lines 7 and 8).

(a) A solution containing 2.2 mM Pb^{2+} and agar is placed in a 5.3-mm inner diameter test tube and allowed to gel, and then a solution of 22.4 mM I^- and agar is poured on top and allowed to gel. The initial values of *S* and Δ are 1007 and 9.0 mM, respectively. Because Δ is positive, the precipitated lead iodide appears in the lead solution. (See, however, the note in ref 16.) Measurements on transmitted light through the system are shown in Figure 7. In panel A of that Figure, we plot the intensity of transmitted light versus the distance from the junction of the two reactant solutions 16 h after initiating the experiment (the joining of the two reactant solutions). At the origin where the two solutions meet, there is a band of PbI_2 indicated by the gray area. The broad minimum from about 3−6 mm is a region of yellowish colloid that is continuous in space. At 24 h, the sharp minimum at 5 mm shown in panel B is due to a clearly

Figure 6. Structures forming from initially homogeneous lead iodide sol in gel (produced by mixing 9 mM KI with 2.25 mM $Pb(NO_3)_2$ in a 0.5% agar−agar solution), on top of which was placed a solution containing KI with concentrations (left to right) of 0.9, 4.5, and 9 mM. Diffusion of the electrolyte occurs out of the gel up into the supernatant solution (from ref 53, Figure 5).

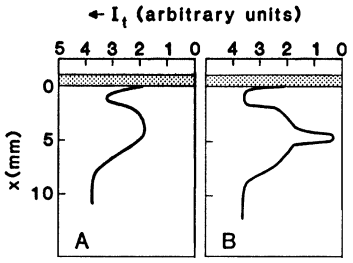

Figure 7. Early stages of precipitation patterns in an experiment with $S = 1007$ and $\Delta = 9$ mM represented by plots of the intensity of transmitted light I_t vs space coordinate *x*. Times after the start of the experiment: (A) 16 h, (B) 24 h (adapted from Figure 3 in ref 38).

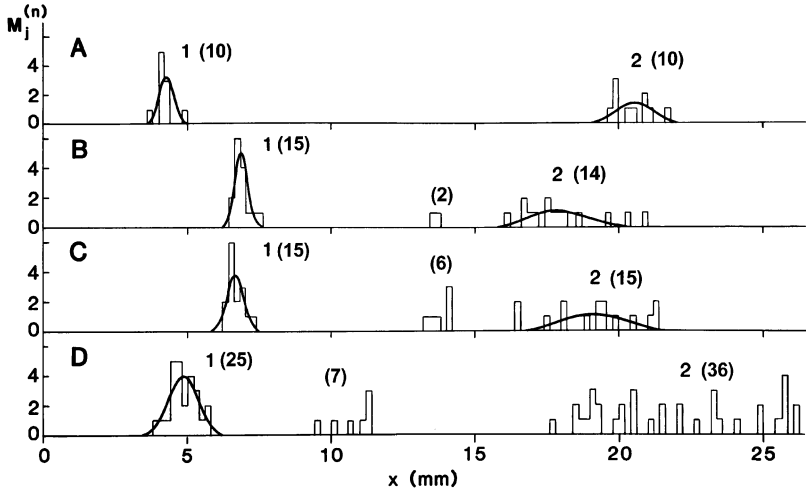

Figure 8. Histograms of band locations for a series of tubes prepared with $S = 1300$ fixed and $\Delta = 108$ mM (A), 2.4 mM (B), 0.9 mM (C), and 0 mM (D). The histograms are labeled with the respective band number $n = 1$ or 2. The numbers in parantheses for band $n = 1$ correspond to the total number of prepared tubes in the specific system. Differences in these numbers for $n = 2$ are due to the formation of two rings with relatively narrow spacing, both contributing to one common histogram. The numbers between $n = 1$ and 2 indicate faint rings that do not always form. To some of the histograms a Gaussian distribution function is fitted (from ref 38).

visible band of precipitate. The band is formed within 24 h in a region in which nucleation has occurred prior to 16 h. Band formation occurs with a reduction of colloid on either side of the band. The time necessary for band formation is much too short for a significant amount of colloid diffusion. Rather, colloid on either side of the band dissociates to monomer electrolyte, and the ions diffuse. This is a typical case of Ostwald ripening with diffusion that leads to a Turing instability,[54,55] also called a focusing mechanism in the literature.

(b) The second experimental result from ref 38 (Table 1, line 8) is shown in Figure 8. Here the value of S is 1300. $\Delta = 108$ mM in panel A, 2.4 mM in B, 0.9 mM in C, and 0 mM in D. At fixed S, decreasing Δ, and decreasing gradient (increasing distance x from the initial electrolyte junction), there is an increase in the broadening of the stochastic placement of the positions of the bands of precipitate. Furthermore, in the spatial regions normally assigned to the second band, there often appear two bands at closely adjacent locations instead of only one, and faint structures exist that are not easily recognizable as a precipitation band.[38] We comment on this later.

(2) During the long-term evolution of a Liesegang experiment, broad precipitation bands (width 4 mm) located relatively far away from the initial electrolyte junction have been shown to split into two narrower bands (Figure 9 and Table 1, line 9 [56]). The edges of the precipitated region were observed to grow faster than the central region during the growth process of the bands (1−2 days), but no measurements were made on the depletion of material in the space between the split bands. This splitting process occurs in a spatial region of low concentration gradients, comparable, for instance, to the region for $x > 18$ mm in Figure 8, panel D, where with some probability two bands instead of one were observed.

(3) In ref 57, there were reported measurements on the temporal and spatial sequences of events in Liesegang ring formation as 5.5 M NH_4OH diffuses into 0.4 M $MgSO_4$ (cf. Table 1, line 10). The initial value of S is 1.01×10^{12}, and $\Delta = 5.1$ M. The results we choose to focus on are shown in Figures 10 and 11. Figure 10 gives plots of measurements of the position of the front of pH 9 at given times as NH_4OH diffuses into $MgSO_4$, the position of the front of turbidity at given times, the time and location of the onset of ring formation as detected by refractive index gradient measurements, and the time and location of the visible appearance of rings. At any given location, the pH front appears first and is then followed by nucleation, colloid formation, and subsequent turbidity. From a region of colloid of nearly constant concentration but in a gradient of OH^- (see curves a and b in Figure 11 that show refractive index gradient measurements), there arises a band of precipitate with an attending depletion of colloidal particles from both sides of the forming band (curves c−f in Figure 11). This depletion must occur, again, by Ostwald ripening, that is, by the dissolution of colloidal particles to the left and right of the forming band and the diffusion of both Mg^{2+} and OH^- toward the forming band, leading to the growth of colloidal particles in the region of the forming band and thus to the band itself. The diffusion of the colloidal particles is too slow in the gel network to account for this process.

For later measurements with similar results on the formation of a region of colloid (turbidity front) prior to the appearance of a band in the silver chromate/dichromate system, see ref 41 and Table 1, line 11.

All of the experiments discussed in section II.C. 1a and b, 2, and 3 are indicative of band growth by a Turing instability based on the auto-catalytic growth of larger colloidal particles (Ostwald ripening)[3,10,11] coupled with diffusion. Band formation arises from a region of continuous colloid of nearly constant concentration and requires some time. This kind of band formation has been demonstrated in numerical studies based on a model of autocatalytic growth of colloidal particles. (See G. Venzl, refs 54 and 55 and also refs 14 and 58.) Venzl's work required a trigger to set off a transition from a slow rate of colloidal growth to a rapid growth of colloid and hence the growth of a band. This trigger seems to be provided in the case in section II.C.3 by attaining a given OH^- concentration, which is essentially determined by the diffusion of OH^-. We calculate the value of x, the position of each band, divided by $t^{1/2}$, where t is the time of formation of the band, and find these ratios to be nearly constant, about 0.43 ± 0.03 mm/min$^{1/2}$. Hence, the trigger necessary for band formation in this Turing instability may well be the attainment of a given OH^- concentration.

The formation of a band by a Turing instability requires the diffusion of ions. In the third band (Figure 11), the diffusion occurs over a distance of about 2 mm, and the diffusion coefficient of $Mg(OH)_2$ is 2×10^{-5} cm^2/s. A crude estimate of

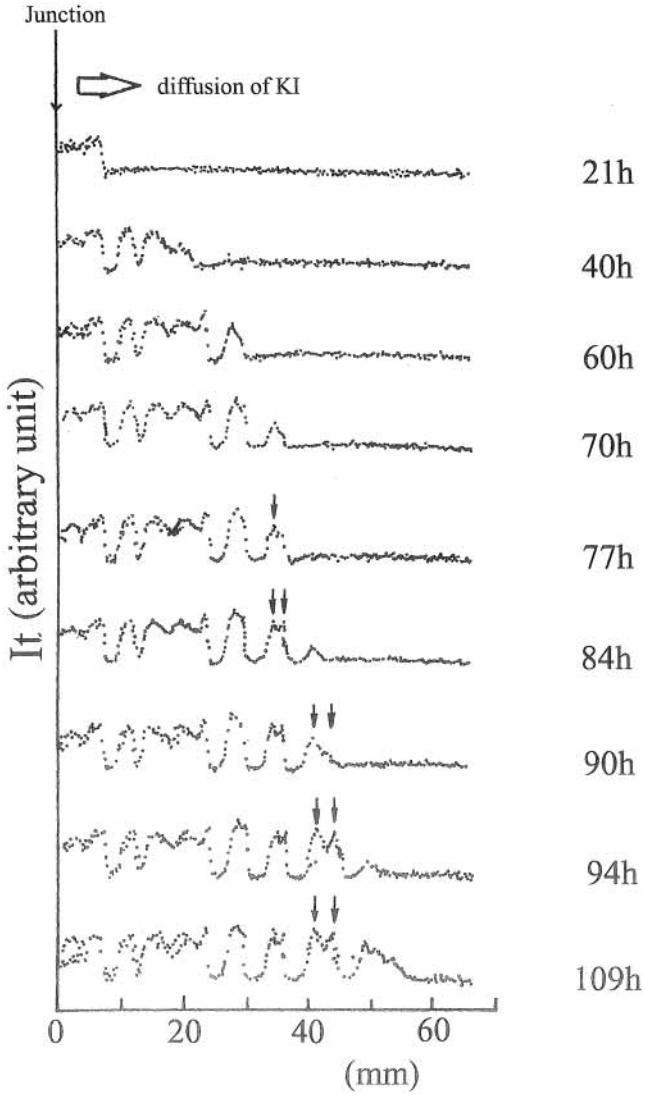

Figure 9. Splitting of precipitation bands of lead iodide. The intensity of transmitted light I_t is plotted vs the space coordinate; the times after the start of the experiment are indicated for each intensity curve. Splitting occurs after 84 h (see arrows). Initial concentrations: outer electrolyte 0.3 M KI, inner electrolyte 0.015 M $Pb(NO_3)_2$ ($S = 1 \times 10^5$, $\Delta = 135$ mM) (from ref 56).

the time necessary for that diffusion to occur (with $x = (Dt)^{1/2}$) is 66 min, compared to the observed time of about 60 min. For other corroborative theoretical evidence for the instability mechanism, see ref 40 cited in the Discussion.

We see that the band-spacing law, position $x \approx t^{1/2}$, is obeyed in the experiments of sections II.C.1.a and II.C.3 and reported previously for many experiments interpreted either by the OP model or the post-nucleation instability hypothesis. Hence, spacing laws are not stringent tests of the mechanism of Liesegang band formation.

In the articles in ref 47, the statement appears repeatedly in footnotes that the theories based on an instability present in the post-nucleation coarsening process cannot explain the regular aspects of the band spacing. Here we have shown by several examples that regular as well as stochastic band formation may occur by a focusing mechanism (instability) from a continuously formed colloid in the presence of a gradient.

The observation in section II.C.1.b of the increasing stochastic placement of precipitation bands with decreasing Δ and also S and a decreasing gradient also requires an explanation based on a Turing instability. For example, the smallest gradient in

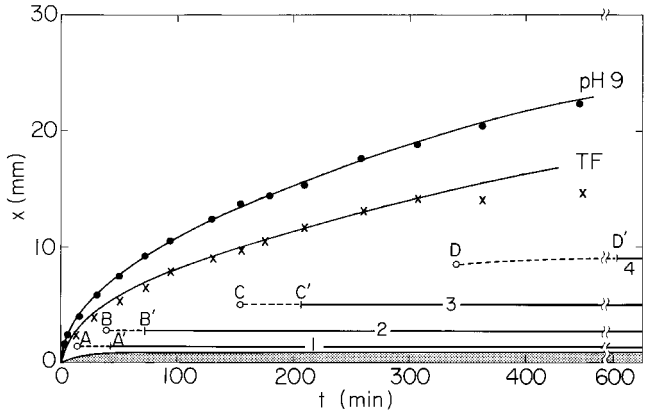

Figure 10. Temporal evolution of the position of the front of pH 9, the front of turbidity (TF), located gradients of refractive index, and visible bands for $Mg(OH)_2$ Liesegang bands with 0.4 M $MgSO_4$ in 9% gelatin and 0.5 M NH_4OH as reagents. The moments of detection of the refractive index gradients are marked by A, B, C, and D, and the moments of the appearance of the four visible rings, by A′, B′, C′, and D′ for the respective ring locations (from ref 57).

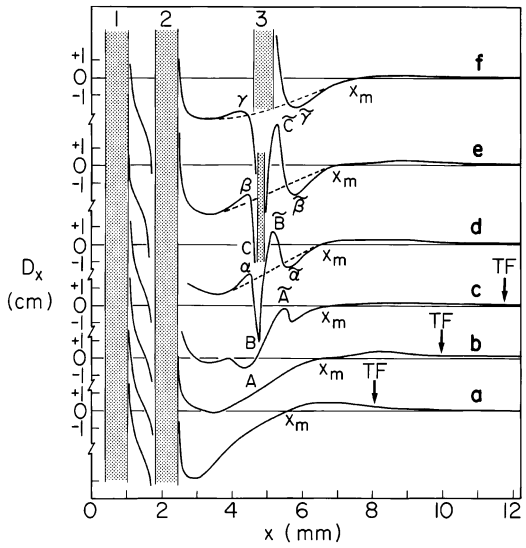

Figure 11. Deflection of a thin laser beam D_x as a measure of refractive index gradients as a function of the x coordinate of a cuvette in which $Mg(OH)_2$ Liesegang bands form with reagents as described in Figure 10. The curves labeled a−f were measured during the following times after the start of the experiment: (a) 107−112 min, (b) 165−170 min, (c) 180−186 min, (d) 195−205 min, (e) 215−225 min, (f) 260−270 min. The origin of the ordinate axis is shifted for each curve. The shaded areas indicate the regions of visible bands with band number 1, 2, and 3; x_m denotes the intersection of the curves with the horizontal axis. The arrows refer to the location of the turbidity front (TF) (cf. Figure 10). For further details, see Figure 8 in ref 57.

Figure 8 is in panel D in the region of 18−27 mm, and there the broadness of the stochastic placement of the bands is the largest. The limiting case of these studies is that of initially uniform systems discussed in section II.A, where structure arises by a Turing instability and is randomly placed (see refs 10, 37, and 51) if not constrained by the geometry of the vessel containing the system (see ref 3).

4. "Typical" Liesegang Experiments. There are many experiments on Liesegang rings, stretching over a period of over more than 100 years, with a typical appearance of band spacing and bandwidths as shown in Figures 12 and 13. In Figure 12, $Pb(NO)_3$ is the electrolyte at high concentration that diffuses into the gel containing KI at much lower concentration ($S = 4.2 \times 10^3$) (ref 43; see Table 1, line 12). For Figure 13, the electrolytes

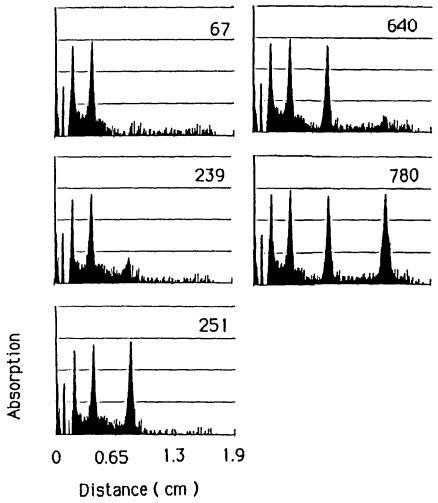

Figure 12. Temporal sequence of scans of the development of the periodic precipitation of lead iodide showing the absorption due to the total concentration of lead iodide along a tube (measured with a 1D photodiode array). Initial concentrations: 0.45 M $Pb(NO_3)_2$ in 1% agarose, 0.01 M KI in 1% agar. The numbers in the upper-right corners denote the time of the scan in minutes after the initiation of the experiment (adapted from Figure 2 in ref 52).

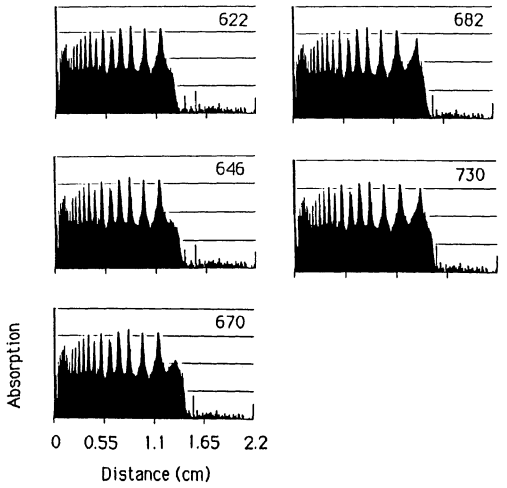

Figure 13. Temporal sequence of scans of the development of periodic precipitation measured in a lead iodide system with initial concentrations of 0.2 M KI in 1% agarose and 0.0045 M $Pb(NO_3)_2$ in 1% agar. The numbers in the upper-right corners denote the time of the scan in minutes after the initiation of the experiment (adapted from Figure 3 in ref 52).

are reversed ($S = 1.7 \times 10^4$). The time scale of intervals between band formation is about 200 min, but the time scale of band formation is shorter, about 20 to 30 min. The spacing time law, in which the position of the *n*th ring is proportional to $t^{1/2}$, is obeyed.

Both Figures show a temporal sequence of scans of transmitted light absorption. The absorption is proportional to the total concentration of lead iodide, which is essentially all in the colloidal state. The system in Figure 12 produces narrow bands with little and in some cases no visible (by eye) colloid formation at any time in the regions between the bands, but with an increasing concentration of KI (i.e., decreasing Δ), nucleation becomes detectable at all distances. When electrolyte concentrations are reversed (Figure 13), one observes well-defined bands forming in the wake of a precipitation front corresponding to the first visual appearance of a yellowish haze. Because subsequent bands are formed sufficiently closely to overlap, there are no clear spaces left between them.

Many of these typical experiments have been interpreted on the basis of the Ostwald−Prager model of periodic precipitation, introduced in section I., but in none of these cases have adequate experiments been made to determne if colloid formation in a broader zone than a Liesegang band preceded band formation.

5. A Continuing Puzzle. In 1962, Higuchi and Matuura[59] (see Table 1, line 13) presented measurements on structure formation in OH^- diffusing into Mg^{2+}, an example of which is given in Figure 14. The system is the same, with still higher concentrations, as that in section II.C.3. In that section, we showed colloid formation of nearly uniform turbidity. In Figure 14, we see a varying Mg^{2+} concentration; unspecified in ref 59 was whether this was in the form of an electrolyte or colloid. The chemical method of analysis in ref 59 may be more precise than the physical methods used in section II.C.2, which showed at best a hint of such variations within the precision of the measurements.

III. Discussion

We have analyzed many cases for which experiments show the applicability of the post-nucleation model. Liesegang rings arise from a region of continuous colloid of nearly constant concentration by Ostwald ripening, a Turing instability. Experiments cited for the applicability of the Ostwald−Prager model, based on supersaturation and nucleation discontinuous in space, have not included measurements probing the possible formation of a continuous colloidal region. Hence, conclusions in favor of the Ostwald−Prager model require more investigation and substantiation.

The ordering of the selected experiments by the quantities S and Δ, defined at the beginning of section II, shows that increasing these quantities in a Liesegang experiment leads to a decreased time of the appearance of bands and decreased band spacing. Decreasing S and Δ leads to an increased stochastic location of the precipitate bands. Structure formation over the entire range of S and Δ seems to be best explained by Turing instabilities.

The bands in a Liesegang experiment carried out in a vessel of test tube dimensions are on a space scale of millimeters to centimeters. Structures in a more limited space, as in a gel layer of millimeter thickness, are on a smaller scale, on the order of 0.2−5 mm. In polymeric film (thickness 0.18 mm), structures are observed on a micrometer scale.[23]

Several attempts have been made in the formulation of theories of Liesegang rings that extend the Ostwald−Prager model[52,60] and that attempt to include both the Ostwald−Prager and the Ostwald ripening (instability) model[45] as well as the transition between these models.[41,61] None seem to fit all of the available experiments. To discuss this transition, Chacron and L'Heureux[61] focus on a phenomenological constant defined in terms of the capillary length w,

$$w = \frac{2v\sigma}{pN_o k_B T}$$

where σ is the surface tension of a precipitate particle, p is a stoichiometric coefficient equal to 2, and v is the molar volume. Another parameter δ, characterizing the thickness of the Gibbs surface but otherwise unspecified, is needed to define the parameter $\Delta = \delta/w$. For $\Delta = 0.16$, they obtain precipitate bands, and for $\Delta = 0.136$, they obtain twin-peaked bands of precipitate. No dependence of any of the quantities, which enter into their Δ, on the concentrations of any species, on S, and on the concentration difference (also called Δ in our work) is taken

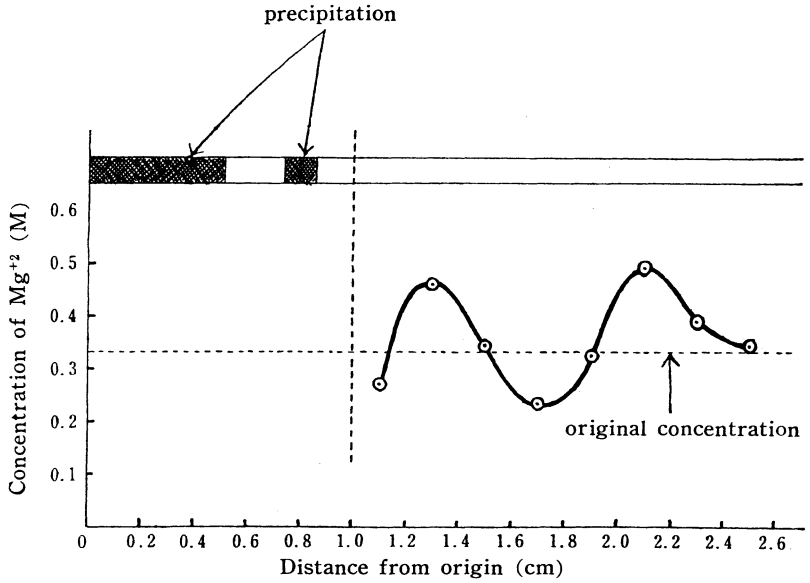

Figure 14. Concentration distribution of Mg^{2+} ions in the gelatin gel before the periodic precipitation of $Mg(OH)_2$ bands takes place, as determined by an EDTA method. Initial concentrations: 11.8 M NH_4OH and 0.33 M $Mg(SO_4)_2$, 10% gelatin (from ref 59).

into account, nor are there predictions of the deposition of colloid from which some time later there emerges a band, as observed in sections II.C.1. and II.C.3.

Krug and Brandtstädter[42] attempt to describe the transition by introducing a nucleation process that leads to very small particles and a stable colloid phase. This leads later to the competitive growth of these particles after an average critical radius is reached. Their equations lead to band formation, and the last band is preceded by a colloidal region from which the next band then arises.

IV. Suggested Experiments

The emphasis of future experiments should lie in the analysis of growth characteristics of individual precipitation regions and their vicinity on microscopic and mesoscopic scales but less on the global description in terms of macroscopic laws. We provide some suggestions for future experiments.

Consider the ion concentration, say, of OH^- in the experiments discussed in section II.C.3. As OH^- diffuses into the region containing Mg^{2+}, its concentration rises until colloid formation occurs. Then, as seen in Figure 11, the measurements of the index of refraction show concentration changes of ions (OH^- and Mg^{++}**)** and of the volume fraction of colloidal $Mg(OH)_2$. The changes in ion concentration may be measurable with ion-specific microelectrodes placed in the region of band growth and in the neighboring regions, where colloidal particles are decreasing in size and ions diffuse to the region of band growth, that is, the region of colloidal growth.[62]

The experimental techniques of light scattering, refractive index measurements, light transmission (spectrophotometry), and chemical analysis of slices of a Liesegang experiment in a tube need to be applied to several systems in a systematic way during the entire period of structure evolution. For example, in Liesegang systems such as the ones shown in Figures 12 and 13, these techniques should be applied to look for evidence of growing colloidal particles prior to band formation in the region of a band and in the interband spaces. The chemical analysis of the slices may provide information about the total concentration of a specific compound (e.g., iodide[53]), but then one needs to determine whether it is present in the form of ions or incorporated into the growing colloidal particles. Separation could be realized by centrifugation of the colloidal particles and analysis of the supernatant liquid as well as by raising the temperature of the slice until the melting of the gel, followed by quick flushing of the liquid containing the ions.

To study the competition between homogeneous and heterogeneous nucleation in the supercooled gradient-free patterns, add a well-defined amount of heterogeneities at the beginning of an experiment.

The process of band splitting (Figure 9) should be monitored continuously during the typically long time of occurrence with a time lapse recorder to obtain information on whether both edges of the band grow faster than the center of the band or the growth of the center is suppressed by the depletion of material. To verify whether band splitting is due to Ostwald ripening, temporal measurements of the particle sizes at the center of the band, preferentially with scattering techniques, are necessary. (There are simulations on the basis of Ostwald ripening that reproduce the measurement of light intensity in Figure 9 well (cf. Figure 11 in ref 56).)

Acknowledgment. We thank H.-J. Krug, H. Brandtstädter, I. L'Heureux, and S. Kai for fruitful discussions. Technical help by S. Tsuji and W. Jantoss is gratefully acknowledged. This work was supported in part by the National Science Foundation.

Appendix A

We give a simple explanation of the difference in appearance of Figures 3A and 4A discussed in section II.A.2 (ref 36). The initial concentration of PbI_2 is 5.2 mM in Figure 3A and 6.4 mM in Figure 4A. The number of particles of average size $\langle R \rangle$ at a given concentration is proportional to that concentration and inversely proportional to $\langle R \rangle^3$. The area projected by these particles considered in a plane is proportional to $\langle R \rangle^2$. The average $\langle R \rangle$ for the 6.4 mM system is 0.8 μm, and for the 5.2 mM system, it is 4.3 μm. Hence, we have the following:

The projected area compared to particles in a 6.4 mM system/ the same for a 5.2 mM system = [6.4/5.2][4.3/0.8] = 6.6. The assumption of all particles being in a plane is likely too severe, but the number of planes is small, probably 2 or 3, and these numbers explain qualitatively the difference in appearance of Figures 3A and 4A.

Appendix B. Estimate of the Probability of Homogeneous Nucleation.

We use the simplest approach of an equilibrium calculation of the probability of a thermal fluctuation of finding a given number of molecules (say PbI_2) in a given volume of a critical size for a stable nucleus. For a brief summary of the calculation, see section IV in ref 63; for basic references, see ref 64. Consider a small volume v in a much larger volume V; let the average number of particles in v be ν. Observe the number of particles in v at regular time intervals τ. The probability of observing n particles in v is

$$W(n) = \frac{e^{-\nu}\,\nu^n}{n!} \tag{A.1}$$

To a good approximation, the recurrence time between two observations of n in v is

$$\Theta_n = \frac{\tau}{[N\,W(n)]} \tag{A.2}$$

The probability of observing n at any one measurement is inversely proportional to the recurrence time.

Let us choose some numbers. Suppose that in the volume V there are 10^{16} molecules. For a concentration of 0.093 M, typical for the experiments discussed in section II.A.3, these molecules occupy a volume of 2.6×10^{-3} cm^3. Suppose we guess that a critical (stable) nucleus contains five molecules. For a density of 0.075 mol/cm^3 for PbI_2, we find the volume occupied by five molecules to be 0.65×10^{-22} cm^3, which equals v. The average number of particles in v is $\nu = 2.5 \times 10^{-4}$. The ratio $V/v = N = 4 \times 10^{17}$. With these numbers, we estimate the recurrence time Θ_5 to be approximately equal to 3 s, and the probability of homogeneous nucleation in this model is substantial. The recurrence time for the nucleation of 10 molecules is drastically longer, 4×10^{21} s, and such nucleation occurs with negligible probability.

References and Notes

(1) For an introduction to the extensive literature, see (a) Liesegang, R. E. *Geologische Diffusionen*; Th. Steinkopf: Dresden, 1913. (b) Hedges, E. S.; Myers, J. E. *The Problem of Physicochemical Periodicity*; Edward Arnold & Co.: London, 1926. (c) Hedges, E. S. *Liesegang Rings and Other Periodic Structures*; Chapman and Hall: London, 1932. (d) Stern, K. H. *Bibliography of Liesegang Rings*; 2nd ed.; U.S. Government Printing Office: Washington DC, 1967. (e) Henisch, H. K. *Crystals in Gels and Liesegang Rings*; Cambridge University Press: Cambridge, U.K., 1988. (f) Ortoleva, P. *Geochemical Self-Organization*; Oxford University Press: Oxford, U.K., 1994. (g) *Chemical Waves and Patterns*; Kapral, R., Showalter, K., Eds.; Kluwer Academic Publishers: Dordrecht, The Netherlands, 1995.

(2) Turing, A. *Philos. Trans. R. Soc. London, Ser. B* **1952**, *237*, 37−72.

(3) Flicker, M.; Ross, J. *J. Chem. Phys.* **1974**, *60*, 3458−3456.

(4) For brevity, we assign symbols to the types of models discussed here, which indicate the names of some of the authors but certainly not all who have contributed to this issue. For the OP model, we cite the work presented in refs 5−9, and for the TI model, that presented in refs 3 and 10−14.

(5) Ostwald, W. *Lehrbuch der Allgemeinen Chemie*; Engelmann: Leipzig, Germany, 1897.

(6) Prager, S. *J. Chem. Phys.* **1956**, *25*, 279−283.

(7) Wagner, C. *J. Colloid Sci.* **1950**, *5*, 85−97.

(8) Keller, J. B.; Rubinow, S. I. *J. Chem. Phys.* **1981**, *74*, 5000−5007.

(9) Smith, D. A. *J. Chem. Phys.* **1984**, *81*, 3102−3115.

(10) Feinn, D.; Ortoleva, P.; Scalf, W.; Schmidt, S.; Wolff, M. *J. Chem. Phys.* **1978**, *69*, 27−39.

(11) Feeney, R.; Schmidt, S. L.; Strickholm, P.; Chadam J.; Ortoleva, P. *J. Chem. Phys.* **1983**, *78*, 1293−1311.

(12) Ross, J.; Arkin, A. P.; Müller, S. C. *J. Phys. Chem.* **1995**, *99*, 10417−10419.

(13) Lovett, R.; Ortoleva, P.; Ross, J. *J. Chem. Phys.* **1978**, *69*, 947−955.

(14) Venzl, G.; Ross, J. *J. Chem. Phys.* **1982**, *77*, 1302−1307.

(15) Kai, S.; Müller, S. C. *Sci. Forum* **1985**, *1*, 9−39.

(16) Commonly, the electrolyte at high concentration is denoted as the "outer" electrolyte that diffuses into the domain initially occupied by the "inner" electrolyte at substantially lower concentration (high Δ), where the bands are later observed to form. We abstain from these notions because at low or zero Δ values bands may form on either side of the initial electrolyte junction, depending sensitively on the diffusivities of the electrolytes and on the external conditions (e. g. the orientation of the tubes with respect to the direction of the gravitational field; cf. Figure 4 of ref 26).

(17) Liesegang, R. E. *Lieseg. Photograph. Archiv* **1896**, *37*, 321−326.

(18) Lloyd, F. E.; Moravek, V. *J. Phys. Chem.* **1931**, *35*, 1512−1564.

(19) Isemura, T. *Bull. Chem. Soc. Jpn.* **1939**, *14*, 179−237.

(20) Morse, H. W.; Pierce, G. W. *Z. Phys. Chem.* **1903**, *45*, 589−607.

(21) Klueh, R. L.; Mullins, W. *Act. Met.* **1969**, *17*, 59−67.

(22) Koenig, A. E. *J. Phys. Chem.* **1920**, *24*, 466. Spotz, E. L.; Hirschfelder, J. O. *J. Chem. Phys.* **1951**, *19*, 1215.

(23) Mueller, K. F. *Science* **1984**, *225*, 1021−1023.

(24) Komatsu, H. *Bull. Jpn. Soc. Appl. Phys.* **1992**, *61*, 830−834.

(25) Jablczynski, C. K. *Bull. Soc. Chim.* **1923**, *33*, 1592−1602.

(26) Müller, S. C.; Kai, S.; Ross, J. *J. Phys. Chem.* **1982**, *86*, 4078−4087.

(27) Droz, M.; Magnin J.; Zrinyi. M. *J. Phys. Chem.* **1999**, *110*, 9618−9622.

(28) Hedges, E.; Henley, R. V. *J. Chem. Soc.* **1928**, 2714−2726.

(29) Packter, A. *Nature* **1955**, *175*, 556−557.

(30) Bull, M. L.; Veil, S. *Compt. Rend.* **1931**, *192*, 682−683.

(31) Ramaiah, K. S. *Proc. − Indian Acad. Sci., Sect. A* **1939**, *9*, 467−478.

(32) Müller, S. C.; Kai, S.; Ross, J. *Science* **1982**, *216*, 635−637.

(33) Raman, S. C. V.; Ramaiah, K. S. *Proc. Indian Acad. Sci., Sect. A* **1939**, *9*, 455−466.

(34) Liesegang, R. E. *Z. Phys. Chem.* **1914**, *88*, 1−12.

(35) Fricke, R.; Suwelack, O. *Z. Phys. Chem.* **1926**, *124*, 359−393.

(36) Hantz, P. *J. Phys. Chem. B* **2000**, *104*, 4266−4272.

(37) Müller, S. C.; Kai, S.; Ross, J. *J. Phys. Chem.* **1982**, *86*, 4293−4297.

(38) Kai, S.; Müller, S. C.; Ross, J. *J. Phys. Chem.* **1983**, *87*, 806−813.

(39) Das, I.; Pushkarna, A.; Bhattacharjee, A. *J. Phys. Chem.* **1991**, *95*, 3866−3873.

(40) Lagzi, I. *Phys. Chem. Chem. Phys.* **2002**, *4*, 1268−1270.

(41) Lexa, D.; Holba, V. *Colloid Polym. Sci.* **1993**, *271*, 884−890.

(42) Krug, H.-J.; Brandtstädter, H. *J. Phys. Chem. A* **1999**, *103*, 7811−7820.

(43) Stern, K. H. *Chem. Rev.* **1954**, *54*, 79−99.

(44) Dhar, N. R.; Chatterji, A. C. *Kolloid-Z.* **1925**, *37*, 2−9. Dhar, N. R.; Chatterji, A. C. *Kolloid-Z.* **1925**, *37*, 89−97. Shinohara, S. *J. Phys. Soc. Jpn.* **1970**, *29*, 1073−1087.

(45) Chernavskii, D. S.; Polezhaev, A. A.; Müller S. C. *Physica D* **1991**, *54*, 160−170. Polezhaev, A. A.; Müller, S. C. *Chaos* **1994**, *4*, 631−636.

(46) Chopard, B.; Luthi, P.; Droz, M. *Phys. Rev. Lett.* **1994**, *72*, 1384−1387.

(47) Antal, T.; Droz, M.; Magnin, J.; Rácz, Z.; Zrinyi, M. *J. Chem. Phys.* **1998**, *109*, 9479−9486. Antal, Z. T.; Droz, M.; Magnin, J.; Rácz, Z. *Phys. Rev. Lett.* **1999**, *83*, 2880−2883.

(48) Castets, V.; Dulos, E.; Boissonade, J.; De Kepper, P. *Phys. Rev. Lett.* **1990**, *64*, 2953−2956.

(49) Ouyang, Q.; Swinney, L. *Nature* **1991**, *352*, 610−612.

(50) Lengyel, I.; Kadar, S.; Epstein, I. R. *Science* **1993**, *259*, 493−495.

(51) Kai, S. In *Spatio-Temporal Patterns in Nonequilibrium Complex Systems*; Cladis, P. E., Palffy-Muhoray P., Eds.; Addison-Wesley: Reading, MA, 1994; pp 445−468.

(52) LeVan, M. E.; Ross, J. *J. Phys. Chem.* **1987**, *91*, 6300−6308.

(53) Flicker, M. R. A Theory of Periodic Precipitation as a Chemical Instability. Ph.D. Thesis, Massachusetts Institute of Technology, Cambridge, MA, 1973.

(54) Venzl, G. *J. Chem. Phys.* **1986**, *85*, 1996−2005.

(55) Venzl, G. *J. Chem. Phys.* **1986**, *85*, 2006−2011.

(56) Kai, S.; Higaki, S.; Yamasaki, H.; Yamada, T. *Trans. IEE Jpn.* **1987**, *107*, 1011−1018.

(57) Kai, S.; Müller, S. C.; Ross, J. *J. Chem. Phys.* **1982**, *76*, 1392−1406.

(58) Venzl, G.; Ross, J. *J. Chem. Phys.* **1982**, *77*, 1308−1313.

(59) Higuchi, H.; Matuura, R. *Mem. Fac. Sci., Ser. C.5, Kyushu University*, **1962**, 33−42.

(60) Dee, G. T. *Physica D* **1986**, *23*, 340−344.

(61) Chacron, M.; L'Heureux, I. *Phys. Lett. A* **1999**, *263*, 70−77.

(62) Research on this subject is being initiated by Professor Joel Karty, ELAN University, and John Ross.

(63) Mori, E.; Ross, J. *J. Phys. Chem.* **1992**, *96*, 8053−8060.

(64) See refs 17−19 in ref 63.